Energy & Environmental Science

www.rsc.org/ees

PAPER

Matrix-embedded silicon quantum dots for photovoltaic applications: a theoretical study of critical factors

Jun-Wei Luo,* Paul Stradins and Alex Zunger

Si Quantum dots (QD's) are offering the possibilities for improving the efficiency and lowering the cost of solar cells. In this paper we study the PV-related critical factors that may affect design of Si QDs solar cell by performing atomistic calculation including many-body interaction. First, we find that the weak absorption in bulk Si is significantly enhanced in Si QDs, specially in small dot size, due to quantum-confinement induced mixing of Γ-character into the X-like conduction band states. We demonstrate that the atomic symmetry of Si QD also plays an important role on its bandgap and absorption spectrum. Second, quantum confinement has a detrimental effect on another PV property – it significantly enhances the exciton binding energy in Si QDs, leading to difficulty in charge separation. We observe universal linear dependence of exciton binding energy *versus* excitonic gap for all Si QDs. Knowledge of this universal linear function will be helpful to obtain experimentally the exciton binding energy by just measuring the optical gap without requiring knowledge on dot shape, size, and surface treatment. Third, we evaluate the possibility of resonant charge transport in an array of Si QDs *via* miniband channels created by dot-dot coupling. We show that for such charge transport the Si QDs embedded into a matrix should have tight size tolerances and be very closely spaced. Fourth, we find that the loss of quantum confinement effect induced by dot-dot coupling is negligible – smaller than 70 meV even for two dots at intimate contact.

I. Introduction: The need to find a window of opportunity when using quantum dots for solar cells

Zero-dimensional (0D) Quantum-dots (QD's) have been advertised to have two types of advantages over one-dimensional (2D) films or three-dimensional (3D) bulk crystals in the functioning of PV solar cells.[1–3] (i) *Effects or properties that already exist in ordinary thin-films or crystals, but QD's offer tunability or better control of these properties.* For example, (a) when using films or

National Renewable Energy Laboratory, Golden, Colorado, 80401, USA

crystals to make multi-junction solar cells, one faces the issue of careful selection of available bulk layer materials to obtain the desired sequence of bandgaps. These layers have to be matched structurally (as in high-efficiency epitaxial cells) and be compatible both chemically and thermally during growth process of the whole device. In contrast, a multi-junction solar cell based on QD's could use the same chemical dot (*e.g.*, Si) with different sizes in different adjacent layers tuning the gap by quantum confinement. In this case, essentially the same growth and assembly process can be used for the different layers. This could allow a large number of different band-gap layers to be

Broader context

Silicon in bulk crystalline form has been the working horse for photovoltaic (PV) solar energy conversion, but recently, other forms of silicon have been considered, most notably, Si in nanostructure form. It has been proposed that a number of "smallness" effects will be conducive to Si PV, including rectification of the most outstanding problem that bulk Si – its absorption edge at 1.1 eV (1127 nm) – has a too long wavelength and its optical transition at threshold is forbidden, forcing rather thick (thus, expensive) Si layers in PV cells. Other smallness-related advantages of Si include the possibility of creating different layers with different absorption thresholds, thus affording a "tandem", multi-color absorbing cell. Such considerations readily reveal that capitalizing on nano effects involves optimization of counter-indicated properties: If the dots are too small they will have too large electron hole binding, inhibiting their dissociation; if they are too big, nano effects will be lost in favor of bulk effects, *etc.* This paper shows how modern electronic structure theory of nanostructures applied to Si, clarify the nature of the "windows of opportunity" that exist in these various counter-indicated physical properties including size, shape, interdot geometries and the nature of the matrix around the dot.

current-matched to the solar spectrum, raising conversion efficiencies. (b) Light trapping in an active layer of assembled QDs can be realized more efficiently than in traditional PV due to simple, low temperature cell layer assembly on textured substrates (*e.g.*, from nanoparticle inks). (c) Radiation tolerance of 0D QD structures was recently found to be two orders of magnitude higher than that of 2D quantum wells,[4] due to the quantum confinement in all three dimensions. Thus, longer lifetimes of QD PV optoelectronics are expected when used in space applications.

Another class of advantages of QD for solar cells involves (ii) *effects or properties that are quantitatively absent in ordinary thin-films or crystals*. This includes effects such as the existence in QD's of significant electron-hole (excitonic) binding, impeding unipolar transport, and the prospect of obtaining high yield from impact ionization, permitting one to achieve 2 or 3 electron-hole pairs from a single, high-energy photon *via* multiple-exciton generation (MEG) process.[1,5] Common to type (i) and type (ii) strategies of using QDs for solar cell architecture is the need to achieve a "window of opportunity" in geometric parameter space. The reason for this is as follows. Combining adequate optical absorption and efficient carrier conductivity in QDs embedded in a matrix requires high density (3D) assembled dots. If the distance between the dots becomes, however, "too short", the assembly will lose the quantum-confinement virtue of the dot, and along with it the quantum-size tunability of the relevant properties, as well as the factors enhancing MEG in dots (if they exist). At the other extreme, if the distance between dots is "too large", the assembly will have vanishing inter-dot wavefunction overlap and exhibit strong electron-hole (exciton) binding, potentially inhibiting carrier conductivity and reducing their collection. The proposition of finding the right "window of opportunity" in 3D packing of dots to the benefit of solar cells is potentially nontrivial, because the effects involved are quantal. In effect, we are trading the difficulty of packing chemically and structurally dissimilar compounds (attendant upon ordinary multi-junction multi-material III–V crystalline solar cells) with the difficulty of finding optimal 3D architecture of electronic confinement that is compatible with inter-dot electronic communication (in 3D QD arrays).

Performing such an optimization experimentally faces the well-known difficulties of having to establish the particle passivation and transport by controlling the QD growth and tuning the surface chemistries for different QD sizes and geometries. Thus, the effects of 3D geometry might be obscured by size, shape, and inter-dot-distance distributions as well as by surface/interface defects of the dots. An alternative approach is discussed here: *use of theory to look for optimum.*

In the past years reliable theoretical tools have been developed and tested for describing the electronic properties of QDs and their assemblies from the atomistic point of view.[6–10] No longer it is necessary to use the effective-mass based (continuum) approximations, with their significant flaws[6–10] for describing electronic levels, or to compromise on using continuum elasticity to describe strain in small particles.[11] Unlike the (atomistic) local-density-approximation (LDA) methods,[12,13] the theory discussed here is free from the well-known LDA errors on band gap and effective-masses, both rather detrimental to obtaining a physically correct description of quantum confinement.[9,14] In the modern theory of

QDs one includes a rather complete description of single-particle effects[6–10] (multi-band interaction; multi-valley coupling; spin–orbit interaction; direct coupling of atomistic strain to the electronic manifold; surface or interface effects), as well as many-particle effects[15] (electron-hole excitonic effects; impact-ionization). Such an approach will help us to understand the origin of the challenges encountered in experimental work on solar cells and field-effect transistors (FETs) based on Si quantum dots.

By modifying the QD size, the QD symmetry, the QD-to-QD size fluctuation, their separation, as well as the electronic barrier posed by the matrix material, we address the following PV-related questions: (i) Does quantum-confinement mix sufficient Γ-character into the otherwise indirect (*X*-like) CBM of Si to give it direct characteristics. (ii) Given that excitonic effects are an inevitable consequence of confinement of electrons and holes in small QD volumes, and given that dissociation of such excitons is a pre-requisite for PV to produce current, one needs to determine the magnitude of the excitonic binding energy as a function of the 3D architecture. (iii) To what extent is quantum confinement lost or modified by 3D packing of Si QDs and moving them closer to each other, to the point of intimate contact. (iv) What is the extent of communication between neighboring dots (charge transport), as witnessed by their wavefunction overlap, energy level splitting, and emergence of minibands, as function of their separation and band offsets with respect to the matrix. (v) What is the effect of size fluctuations and QD symmetry changes between neighboring dots (to be inevitably expected in a realistic PV absorber material) on the dot-dot communication, and as possible cause for carrier localization.

By addressing the questions above, we present a systematic and quantitative study of critical factors that need to be considered in designing Si QD solar cells. (i) We show that optical absorption, governed by relatively weak indirect transitions in bulk c-Si, is exponentially enhanced at small QD sizes because of the strong coupling between the states from the edges and the center of the Brillouin zone. (ii) Exciton binding energy in Si QDs is found to be quite large (∼100 meV) and should be taken into account in cell design. (iii) Bringing dots intimately close results in a little loss of quantum confinement. (iv) Very close contact (from intimate to couple Å) between the neighboring dots is necessary for the dot-dot coupling and ultimately, realization of transport minibands. This distance dependence is particularly pronounced for dots embedded in a large-gap insulating matrix, and for HOMO levels. Coupling decreases with increasing the dot size. (v) Size fluctuations and symmetry variations in the dots introduce disorder in the energy landscape of the QD array, similarly reducing the dot-dot coupling.

II. Theory approach to realistic description of electronic properties of 3D assemblies of Si dots

The atomistic calculations of the electronic structure of Si QDs were performed in two steps (ref. 9,15,16).

A. In the first step, the single-particle electron states of Si QDs are obtained from direct-diagonalization of the Schrödinger equation describing the QD as a giant molecule,[9,16]

$$\left(-\frac{\hbar^2}{2m}\nabla^2 + V(\mathbf{r}) \right)\psi_i(\mathbf{r}, \sigma) = \varepsilon_i\psi_i(\mathbf{r}, \sigma), \tag{1}$$

where $\{\varepsilon_i, \psi_i(\mathbf{r}, \sigma)\}$ are energy and wavefunction of state i with spin σ, m is the bare electron mass, and $\hbar$ is the Planck constant. The QD potential $V(\mathbf{r})$ is a superposition of screened atomic potentials $\hat{v}_\alpha$ of atom type α located at atomic site $\mathbf{R}_{n,\alpha}$:

$$V(\mathbf{r}) = \sum_{n,\alpha} \hat{v}_\alpha(\mathbf{r} - \mathbf{R}_{n,\alpha}). \quad (2)$$

The process of the first step is schematized in Fig. 1. The key to the correct description of electronic states are potential $\hat{v}_\alpha$ containing in QD all electronic structure effects without correlation (which comes in the second step): spin–orbit coupling,[17] strain, inter-band (holes/electrons) coupling,[18] inter-valley ($\Gamma - X - L$) coupling, effects of shape and size, and atomistic symmetry.[18] The indices (α, n) extend over the Si QD and the barrier materials. The shapes of the pseudopotential $\hat{v}_\alpha(q)$ of one Si atom and one dot matrix atom is shown in Fig. 1 (a) whereas the sum $V(\mathbf{r})$ of a Si QD is shown in Fig. 1(b). The screened atomic potentials $\hat{v}_\alpha$ were fitted to experimental transition energies, effective masses, and deformation potentials of bulk Si.[14,19]

Given the difficulties of a small basis-set $\mathbf{k} \cdot \mathbf{p}$ to properly recognize the atomistic symmetry ("farsightedness of $\mathbf{k} \cdot \mathbf{p}$"[9,10]), the proper rendering of the electronic structure by $\mathbf{k} \cdot \mathbf{p}$ can be challenging. The atomistic screened pseudopotential approach naturally captures the atomistic symmetry of the system, multi-band, inter-valley and spin–orbit interactions. In contrast to LDA method which had been extensively used to calculate the

electronic structure of small Si QDs and Si nanowires,[20,21] the overestimation of effective masses ($\sim$40%) and underestimation of bandgap ($\sim$60%)[12,13] are corrected in the current atomistic screened pseudopotential method by fitting them to experimental values.[14] To mimic the effects of organic ligands, which are often used to passivate the surface of colloidally-grown QD's, we surround the Si QDs by a fictitious, lattice-matched barrier material having a wide band gap and large type-I band offsets with respect to bulk Si. Hence, the Si QDs calculated in this paper are a strain- and defect-free system. Two types of matrix materials were fitted for Si QDs to reproduce the experimentally measured bandgap of Si QDs passivated by hydrogen[22] or embedded in SiO$_2$ matrix.[22]

The Schrödinger equation [eqn (1)] is solved by expanding the QD electron states in a plane-wave basis set, and selectively calculating the band-edge states using the folded-spectrum method.[23] The computation capacity of our atomistic method is aggressively extended from <1000 atoms of LDA[21,20] (and <100 of atoms using the GW and Bethe-Salpeter method[10]) to up to millions of atoms with the present method.

The QD wave functions of eqn (1) can be analyzed in reciprocal space by projecting them on the bulk Si wave functions, i.e. $\psi_i(\mathbf{r}, \sigma) = \sum C_i(n, \mathbf{k})\phi_{n,\mathbf{k}}(\mathbf{r}, \sigma)$, and summing over the coefficients $C_i(n, \mathbf{k})$ to obtain the projection of the QD state i on each $\mathbf{k}$ point in the bulk Brillouin zone:

$$P_i(\mathbf{k}) = \sum |C_i(n, \mathbf{k})|^2. \quad (3)$$

B. In the second step, once the single-particle states are found, the excitonic energies and wave functions including many-body interaction are calculated in the framework of the configuration-interaction (CI) scheme.[15] In this approach, the excitonic wave functions $\Psi^{(i)}$ are expanded in terms of single-substitution Slater determinants $\Psi_{v,c}$, constructed by promoting an electron from the occupied single-particle state v to the unoccupied single-particle state c:

$$\Psi^{(i)} = \sum_{v=1}^{N_v} \sum_{c=1}^{N_c} C_{v,c}^{(i)} \Psi_{v,c}. \quad (4)$$

The coefficients $C_{v,c}^{(i)}$ of the CI expansion are calculated by diagonalizing the CI Hamiltonian for a single exciton:

$$H_{vc,v'c'} \equiv \langle \Psi_{v,c}|H_{CI}|\Psi_{v',c'}\rangle = (\varepsilon_c - \varepsilon_v)\delta_{v,v'}\delta_{c,c'} - J_{vc,v'c'} + K_{vc,v'c'}, \quad (5)$$

where the Coulomb and exchange integrals $J_{vc,v'c'}$ and $K_{vc,v'c'}$ are respectively given by

$$J_{vc,v'c'} = e^2 \sum \iint \frac{\psi_v(\mathbf{r},\sigma)\psi_c(\mathbf{r}',\sigma')\psi_{v'}(\mathbf{r},\sigma)\psi_{c'}(\mathbf{r}',\sigma')}{\bar{\varepsilon}(\mathbf{r},\mathbf{r}')|\mathbf{r} - \mathbf{r}'|} d\mathbf{r}d\mathbf{r}' \quad (6)$$

$$K_{vc,v'c'} = e^2 \sum \iint \frac{\psi_v(\mathbf{r},\sigma)\psi_c(\mathbf{r}',\sigma')\psi_{c'}(\mathbf{r},\sigma)\psi_{v'}(\mathbf{r}',\sigma')}{\bar{\varepsilon}(\mathbf{r},\mathbf{r}')|\mathbf{r} - \mathbf{r}'|} d\mathbf{r}d\mathbf{r}' \quad (7)$$

The Coulomb potential in eqn (6) and (7) is screened using a position-dependent and size-dependent screening function $\bar{\varepsilon}(\mathbf{r}, \mathbf{r}')$ [CI]. The Slater determinants of eqn (4) are built using 18 valence (including S, P, and D orbital characters of envelope function) and 18 conduction (including S and P orbital characters) band states.
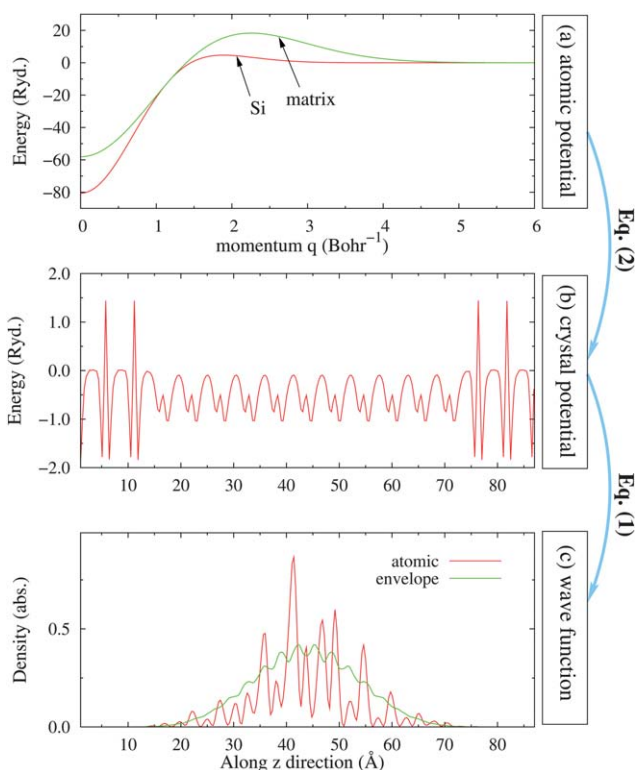
Fig. 1 (a) Single-atom and (b) single-dot pseudopotential and (c) ensuing dot wavefunction. The QD potential $V(\mathbf{r})$ in (b) is a superposition of screened atomic potential $\hat{v}_\alpha$ (here in momentum space) in (a) by solving eqn (2). The wavefunction is obtained by solving eqn (1) once one has crystal potential $V(\mathbf{r})$.

The *excitonic gap* (or exciton transition energy) E_X[24] is approximately the difference in total energy of a QD occupied by an electro-hole pair having as a dominant configuration an electron in the lowest unoccupied molecular orbital (LUMO) e_0 and a hole in the highest occupied molecular orbital (HOMO) h_0 and a QD in the ground state,

$$E_X = E_{1,1}(e_0^1, h_0^1) - E_{0,0}. \qquad (8)$$

Here $E_{1,1}(e_0^1, h_0^1) = \varepsilon_{e_0} - \varepsilon_{h_0} - J_{h_0 e_0, h_0 e_0} + K_{h_0 e_0, h_0 e_0}$, and $J_{h_0 e_0, h_0 e_0}$ and $K_{h_0 e_0, h_0 e_0}$ are the Coulomb and exchange energies between electron and hole, respectively.

The *exciton binding energy* E_b[24] is the difference between the total energy of a system consisting of two infinitely separately identical dots, one with a hole in level h_0 and the other with an electron in level e_0, and the total energy of a quantum dot with an exciton:

$$E_b = E_{1,0} + E_{0,1} - E_{1,1} - E_{0,0}, \qquad (9)$$

where $E_{1,0}$ stands for $E_{1,0}(h_0^0 e_0^1)$, and $E_{0,1} = E_{0,1}(h_0^0, e_0^1)$, and $E_{1,1} = E_{1,1}(h_0^1, e_0^1)$. Besides, a small term called correlation energy $E_{corr.}$ arising from the configuration mixing between $(e_0^1 h_0^1)$ and other higher energy configurations, which is actually included in the present calculation, is neglected in the above definitions of E_X and E_b. We find that E_b is convergence within 1 meV for the CI basis set used in the present calculations.

The *optical absorption spectrum* $I(E)$ in single-particle basis is calculated, considering interband transitions, by using the dipole transition matrix $M_{v \to c} = \langle \psi_v(\mathbf{r}) | \hat{p} | \psi_c(\mathbf{r}) \rangle$,

$$I(E) = \sum_v \sum_c |M_{v \to c}|^2 exp\left[-\left(\frac{E - E_{vc}}{\lambda} \right)^2 \right], \qquad (10)$$

where $E_{vc} = E_c - E_v$ is the transition energy from valence band v to conduction band c and λ represents the spectral line broadening. Eqn (10) gives the absorption in single-particle limit (*e.g.* no Coulomb interaction). To account for excitonic effects, we use excitonic wavefunctions (eqn (4)) to calculate optical absorption (Fig. 5, 7, 8 and 12).

III. Results

A. Energy levels *vs.* dot-matrix band offset in a single Si dot

Ligands at the QD surface passivate the surface dangling bonds, shifting the surface states out the bandgap into the bands. In the present work the Si QDs are embedded in two types of matrix, which has same lattice constant as bulk Si (strain-free), to mimic the Si QDs passivated by hydrogen and embedded in SiO_2 matrix, respectively. The energy level diagrams for a Si QD embedded in two types of matrix, respectively, are shown in Fig. 2. Among the band edges of bulk Si given in Fig. 2(c), Fig. 2(a) shows the electron levels of the Si QD embedded in the $E_g = 3.2$ eV small-gap matrix (SGM) which has conduction and valence band offsets of 1.07 and 1.0 eV, respectively, with respective to bulk Si, while Fig. 2(b) shows the results for the QD embedded in the $E_g = 5.9$ eV large-gap matrix (LGM) which has the conduction and valence band offsets of 2.77 and 2.0 eV, respectively. The SGM was fitted to mimic effect of the SiO_2
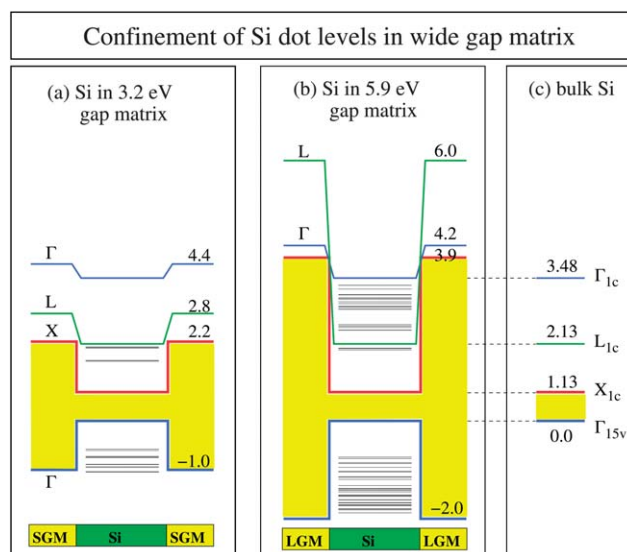
Fig. 2 Calculated band alignment of 2 nm diameter Si quantum-dot (indicated by green area) embedded in two types of model wide-gap material (indicated by yellow area). The model matrix in panel (a) is a small gap matrix (SGM) with $E_g = 3.2$ eV and in panel (b) is a large gap matrix (LGM) with $E_g = 5.9$ eV. Panel (c) is band edges of bulk Si. Horizontal black lines in (a) and (b) denote confined energy levels of Si quantum-dot. The energy values are given in eV.

matrix and the LGM was fitted to mimic the hydrogen ligands on the electron states of the Si QDs.[25] Both effective masses and band offsets play important roles to determine the quantum confinement of size-confined electron states inside the QD.[26] Hence, it is not surprising that the SGM barrier has a much smaller bandgap than the real SiO_2 ($E_g \sim 9$ eV) but reproduces well the bandgap of Si QDs embedded in SiO_2 matrix.
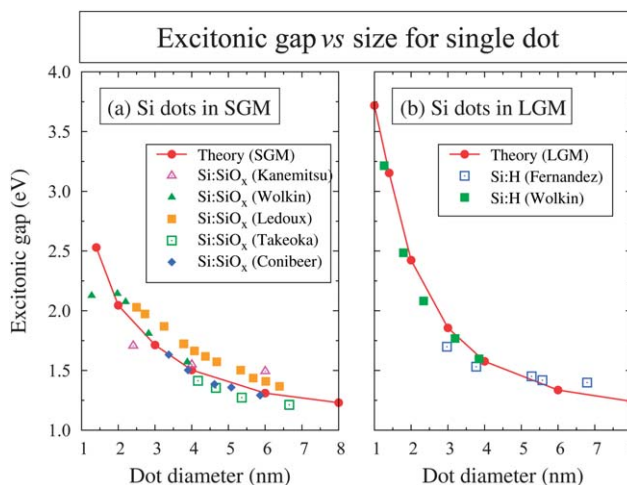
Fig. 3 Atomistic pseudopoential-calculated excitonic gap [eqn (8)] of single Si QDs embedded in (a) a small-gap matrix (SGM) and (b) a large-gap matrix (LGM) in comparison with experimental values as a function of dot size. Experimentally measured Si QD samples were synthesized by different methods and can be sorted into (b) hydrogen passivated oxygen-free Si QDs by Wolkin *et al.*[22] and Fernandez *et al.*;[27] and (a) Si dangling bonds passivated by Si-oxide by Wolkin *et al.*,[22] Takeoka *et al.*,[32] Conibeer *et al.*,[31] Kanemitsu *et al.*;[30] and by Ledoux *et al.*[28]

Fig. 3 shows the calculated excitonic gap [eqn (8)] of Si QDs embedded in SGM (Fig. 3(a)) and in LGM (Fig. 3(b)) as a function of QD size, in comparison with the experimentally measured excitonic gap of Si QDs embedded in various matrix[22,27–29] including hydrogen[22,27] and SiO_2.[22,30–32] We find that the calculated excitonic gap of Si QDs embedded in LGM agrees well with experimental measured gap of hydrogen-terminated Si QDs[22,27] in a wide range of dot size, and the excitonic gap of QDs embedded in SGM lies within the experimental measured gap of Si dot embedded in SiO_2 matrix.[22] As expected from quantum confinement, the excitonic gaps of Si QDs terminated by hydrogen and embedded in SiO_2 are close when dot size is large (small quantum confinement) and is separated gradually as dot size reduced. When dot size is small (<4 nm in diameter), the gap of H-terminated Si QD is distinctly larger than that of SiO_2 terminated.

For an AM1.5 solar spectrum the optimal band gap of the top cell required to maximize conversion efficiency is ~1.7–1.8 eV for a 2-cell tandem with a bulk Si bottom cell and 1.5 eV and 2.0 eV for the middle and upper cells for a 3-cell tandem.[33] According to both experimental measurement and present atomistic calculation, for Si QDs embedded in Si oxide matrix, the upper cell should consist of ~2.8 nm Si QDs layer for 2-cell tandem. Whereas, the top and middle layers should consist of 2 nm and 4 nm Si QDs layers, respectively, for 3-cell tandem.

B. Excitonic electron-hole binding energy E_b in a single Si dot

One photon absorbed by a Si QD will generate one or more electron-hole pairs (excitons). Before the electrons and holes are collected at positive and negative electrodes, one has to separate the electron-hole pair, overcoming the exciton binding energy E_b [eqn (9)].[34,35] The exciton binding energy results from the screened Coulomb interaction between electron and hole; this interaction is enhanced in QDs by the highly confined space in which electron and hole wave functions coexist.[14,15,36]

In Si QDs studied here, the dielectric constant of bulk Si (ε_{Si} = 11.8) inside dot is at least 3 times larger than that of the matrix outside dot (ε_{SiO_2} = 3.9). It was demonstrated[37] that the dielectric constant mismatch between the QD and its surrounding material will form surface image charge and induce non-negligible surface-polarization effects on the carriers, such as the surface-polarization self-energy $\sum_i^{pol}$ of a carrier in the single-particle state i, and the polarization contribution $J_{i,j}^{pol}$ to the Coulomb interaction. However, it was found[37] that the surface-polarization effects on the excitonic gap E_X and exciton binding energy E_b are negligible in the whole range of dot size since the terms $\sum_i^{pol}$ and $J_{i,j}^{pol}$ tend to cancel. In the following we will neglect the effect of surface-polarization.

Fig. 4 shows our calculated exciton binding energy E_b [eqn (9)] for Si QDs embedded in SGM (SiO_2 matrix) and LGM (hydrogen ligands), respectively, as a function of excitonic gap E_X [eqn (8)]. For the case of Si QDs embedded in large-gap matrix, the 2.0 nm diameter dot has binding energy ~300 meV. This is significantly enhanced from 14.3 meV of bulk Si. The binding energy is further enhanced to ~700 meV for dot size 1 nm. Interestingly, the calculated exciton binding energy of all Si QDs lies on a single straight line irrespective of the very different
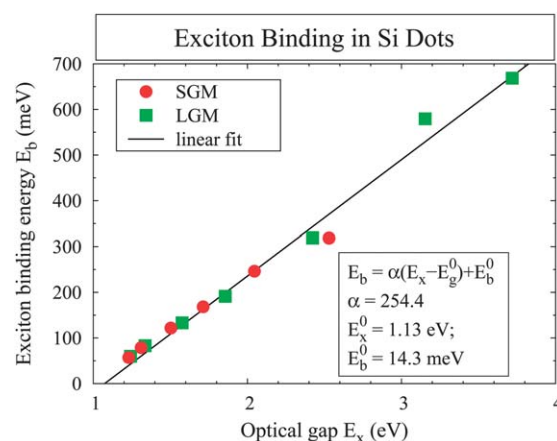

Fig. 4 Calculated exciton binding energy E_b [eqn (9)] of Si dots embedded in a SGM (red circles) and LGM (green squares). All the exciton binding energies E_b lie on a straight line $E_b = \alpha(E_x - E_g^0) + E_b^0$ [eqn (11)], where $\alpha = 254.4$, bulk Si gap $E_g^0 = 1.13$ eV,[19] and exciton binding energy in bulk Si $E_b^0 = 14.3$ meV.[19]

matrix used in the calculations. The linear function of exciton binding energy vs. excitonic gap is:

$$E_b = E_b^0 + \alpha(E_X - E_g^0), \tag{11}$$

here, the coefficient $\alpha = 254.4$ is the only fitted parameter, excitonic gap of bulk Si $E_g^0 = 1.13$ eV, and exciton binding energy in bulk Si is $E_b^0 = 14.3$ meV.[19] This universal linear function is very helpful to obtain experimentally the exciton binding energy of Si QDs by just measuring the optical gap E_X without any knowledge on dot shape, size, and surface treatment.

C. Quantum confinement enhanced absorption intensity in a single dot

Strong absorption intensity in the solar spectrum range 1.5–4.0 eV is desired for the solar cell absorber layer, as this affords thinner absorber layers which provide better carrier collection, are less sensitive to impurities and are more cost effective. Bulk Si, the most prevalent material for current solar cells, is an indirect gap semiconductor – its the absorption is enabled only via low-efficiency phonon-assisted process. Thus, the required minimum thickness of Si layer is limited by this low-efficiency absorption. Fig. 5 shows by blue line (upper line) the calculated zero-phonon absorption intensity of the ground exciton (S_e–S_h transition) as a function excitonic gap for Si QDs embedded in SGM and LGM. As the dot size is reduced, the absorption intensity is enhanced exponentially which agrees with experimental measurement.[38] In order to analyze the leading mechanism for enhanced absorption, we show in Fig. 5 the bulk Γ Bloch component mixed into the QD CBM states with magenta line (lower line). This was calculated according to eqn (3), by projecting its wavefunction to bulk Si Bloch states in the fcc Brillouin zone. The logarithmic Γ-component of the S_e state as a function of optical gap lies also along a straight line (magenta line) with a slightly smaller slope than the line (blue line) of absorption intensity. The slightly larger slope of absorption intensity than that of Γ-component of the S_e state is attributed to
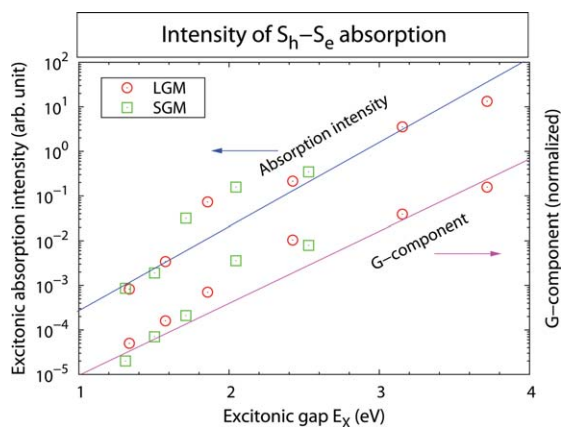
Fig. 5 Calculated absorption intensity [eqn (10)] of the fundamental across-the-gap absorption S_h–S_e transition as a function of the excitonic gap E_X for single Si dots embedded in SGM (squares) and LGM (circles). The right-hand side shows the fraction of Γ-character mixed into the X-like CBM of Si dots.

the contribution of space confinement enhanced electron-hole overlap to the absorption intensity. The LUMO in Si dot is made up from a few bulk Si states including X and Γ and others, so the transition intensity is enhanced relative to pure X as in bulk. Thus, the major mechanism for the significant enhancement of the absorption intensity in Si QDs is due to the relaxation of momentum conversation *via* coupling more Γ-component in the low-lying QD electron states. The exponential dependence of Fig. 5 is similar to the confinement energy dependence of the radiative PL decay rate observed in ref. 39.

We further study the wavefunctions to clarify the above discussion. The single-particle state ladder in energy and corresponding envelope wavefunctions of a 2.0 nm Si QD embedded in LGM are shown in Fig. 6. We find that in conduction band there are six S-like ($L = 0$), 12 P-like ($L = 1$), 18 D-like ($L = 2$), … states derived from six equivalent Δ_X valleys. The S states and P states are well isolated with S–P splitting of $\sim$400 meV and S–D splitting of $\sim$300 meV. In the valence band states of the Si QD, there are three S-like, six P-like, … states derived from close in energy bulk HH, LH, and SO valence bands. The absorption spectrum for 2.0 nm Si QD is shown in Fig. 7. Interestingly, lots of the nominally orbitally-forbidden transitions (*e.g.*, P_h–S_e, D_h–S_e, P_h–D_e) have stronger intensity than the orbitally-allowed S_e–S_h transition. We tentatively attribute these unusually strong transitions to (i) the stronger Γ – X mixing in high-lying P, and D states than in low-lying S states and then it further relax the momentum conservation and (ii) enhanced inter-orbital coupling (S–P, S–D).

D.   Effects of atomic symmetry on absorption spectrum in a single dot

A spherical Si QD with the sphere center at a Si atom has O_h symmetry. If we shift the sphere center away from Si atom to a Si–Si bond, the symmetry of the Si QD is lowered to C_{3v}. Due to the different symmetry groups, the electronic structures of bond-centered and atom-centered Si QDs are expected to be different.[40,41] Such symmetry induced effects on the absorption

spectrum were considered theoretically recently for CdSe[40] and PbSe[41] QDs based on atomistic LDA method and four-band envelope-function approximation, respectively. For CdSe QD, the main effects of symmetry is on the high excitation energy range rather than band-edge transition. Fig. 8 shows the comparison of our atomistic pseudopotential calculated absorption spectrum of atom-centered (top) and bond-centered (bottom) 2.0 nm diameter Si QDs. The absorption spectrum strongly depends on the symmetry of the Si QD. The band-edge S_e–S_h transition of bond-centered Si QD (C_{3v}) is 100 meV red-shifted relative to that of atom-centered Si QD (O_h) having same size as former. The spectrum is more strongly modified at higher excitation energy. This large energy shift can not be explained by the continuum effective-mass approximation because the parameters in the effective-mass Hamiltonian are the same for two spherical Si QDs with same size irrespective of origin. This suggests that even subtle structural variations (induced by different symmetry) produce energy shift of tens meV, which will strongly affect the dot-dot level alignment, introducing energy disorder in the carrier transport path through a dot array as discussed below. This symmetry variation induced disorder in a QD array will reduce the carrier conductivity and efficiency of carrier collection in a cell device. In what follows we study O_h symmetry dots.

E.   Dot arrays: Energy levels *vs.* dot-dot separation

So far we discussed the electronic structure of isolated single QDs in sections A, B, C, and D, we now turn to discuss dot arrays. Fig. 9 shows the real-space wavefunction of band edges (LUMO and HOMO) for an ensemble consisting of eight-dot with same size and same dot-to-dot distance. The wavefunction overlap for LUMO states is apparent. The wavefunction overlap makes the effective size of QDs larger than their isolated counterpart and also enhance the communication between QDs. It is interesting to see to what extent is quantum confinement lost or modified by 3D packing of Si QDs and moving them closer to each other, to the point of intimate contact. To address this question, in what follows we will focus on a dot-dimer system by isolating it from other QDs in an ensemble. Fig. 10(a) schematics a dot-dimer consists of two dots separated by a distance d having D1 and D2 diameters, respectively. If there is strong coupling between these two dots, their wavefunctions overlap [schematized in Fig. 10(b)] and corresponding levels repel [schematized in Fig. 10(c)]. Due to the feature of atomistic discreteness, we can not define two dots in a dot-dimer to have exact size and shape which will introduce its own level splitting that somewhat obscures the real level repulsion. We therefore introduce the LUMO (HOMO) energy difference E_R [Fig. 10(c)] between dot-dimer and isolated dot to reflect the strength of level repulsion. The miniband width Δ in an ordered dot array is approximately two times E_R.
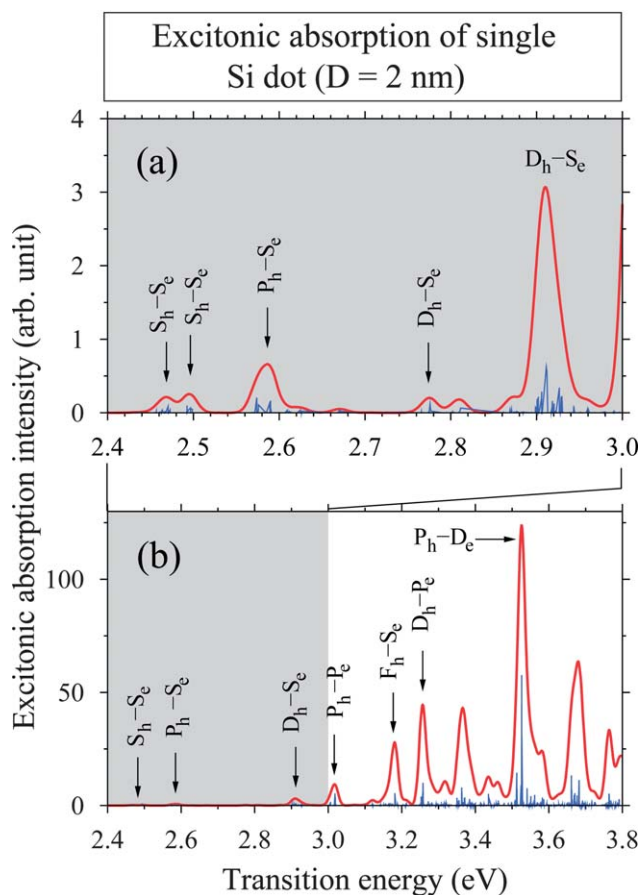
Fig. 11 shows the wavefunction square (partial charge density) of bonding and antibonding of LUMO (left part) and HOMO (right part) as a function of dot-dot distance for Si dot-dimer embedded in SGM. The corresponding optical transition spectra are shown in Fig. 12. The spectrum of Si dot-dimer with face-to-face separation of 7 Å closely resembles that of an isolated Si QD. Changes in the absorption spectra occur only at a face-to-face separations below 4 Å. However, even bringing the dots to

Single dot energy levels and envelope functions
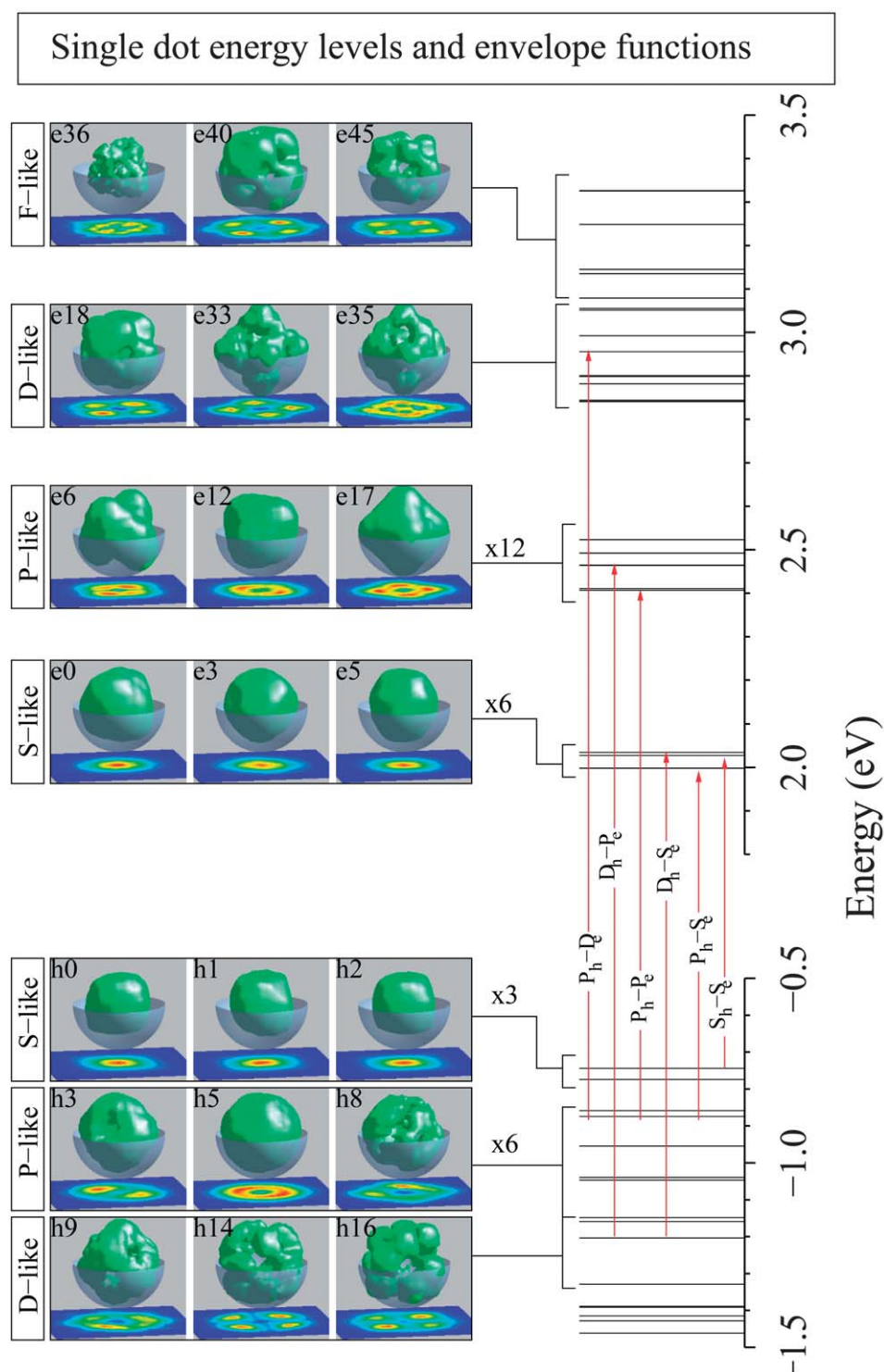
Fig. 6 Left panels show the envelop function $\psi_i(\mathbf{r})$ of eqn (1) of the confined electron levels (top) and hole levels (bottom) for single Si dot with diameter 2 nm embedded in LGM. Right panel shows the transitions from hole states to electron states.

an intimate contact (0 Å) affects the transition energies by only about 50 meV and results in relatively minor widening of the low energy spectral peaks as shown in Fig. 12. This indicates that the quantum confinement is preserved even at intimate proximity, and that level splitting is unlikely to exceed 50–100 meV. We note that in Si QD arrays, the experimental measurements of
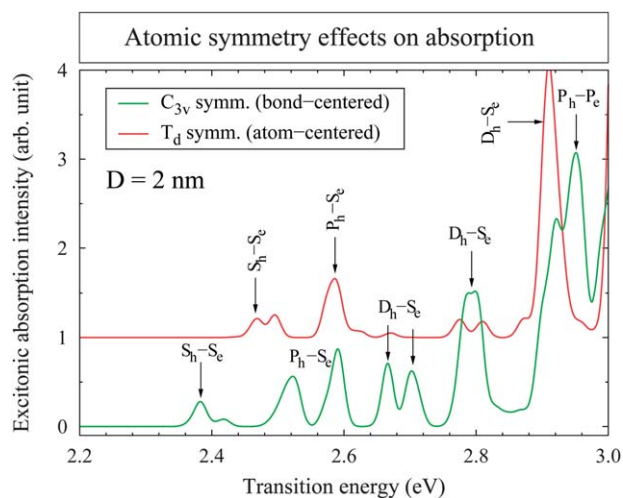
absorption spectra yield smooth energy-dependency without peaks such as in Fig. 12. Since these measurements are typically performed on either isolated dots in solution or on Si QDs in SiO$_2$ matrix separated by about 1 nm, we conclude that size, shape, and symmetry-related energy level fluctuations of the current state-of-the-art Si QDs likely exceed 100 meV making

2552 | *Energy Environ. Sci.*, 2011, **4**, 2546–2557

This journal is © The Royal Society of Chemistry 2011

Fig. 7 Calculated excitonic absorption spectrum [eqn (10)] of single Si dot with diameter 2 nm embedded in a large-gap matrix. (a) is absorption spectrum in a smaller energy range (zoom in). The many-body interaction was taken into accounting by configuration–interaction (CI) method with a basis of 36 electron states (72 including spin) and 32 hole states (64 including spin). Arrows denote the transition peaks between hole (h) and electron (e) with S, P, or D envelope function. The blue vertical lines denote the absorption spectrum without broadening.

Fig. 8 Comparison of excitonic absorption spectrum [eqn (10)] for single Si dot (D = 2 nm) with quantum-dot centered on one Si atom (T_d symmetry, red line) and centered on the Si–Si bond (C_{3v} symmetry, green line). Both T_d symmetry dot and C_{3v} symmetry dot are cut out by a sphere with diameter 2 nm and embedded in large-gap matrix. The vertical labels are for transition peaks of T_d symmetry dot and horizontal labels for transition peaks of C_{3v} symmetry dot.
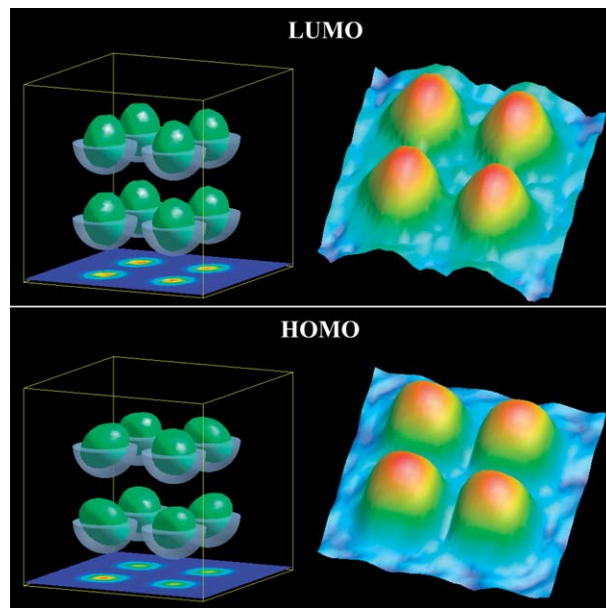
Fig. 9 Wavefunction square (partial charge density) of LUMO (top) and HOMO (bottom) for a Si eight-dot array with 6 nm diameter dots and 1 nm face-to-face distance.

the structure of the spectrum unobservable. This is consistent with Fig. 8 and with Fig. 3 assuming 10% size variation.

The level repulsion E_R (which is related to half the miniband width in an ordered dot array) of LUMO and HOMO is calculated in Fig. 13 for Si dot-dimer embedded in SGM and LGM. It is plotted as function of face-to-face separation d in the Si dot-dimer. The results of Fig. 13 (red curve, dimer of two almost identical Si dots) demonstrate that even for zero separations, the level half-splitting (level repulsion E_R) due to dot-dot interaction is only about 60 meV. This is comparable with disorder energies introduced by symmetry, shape, and size variations as discussed above. The level splitting exponentially decays with increasing the dot-dot separation. Moreover, the splitting is further reduced, to less than 10 meV, for larger size 4 nm dots dimer (black curve). The observed scatter in the data away from the trends is due to the different atomic symmetry of dots (T_d *vs.* C_{3v}). Fig. 13 shows that the level splitting and thus, miniband formation, effectively ceases at face-to-face separations greater than 5 Å for low-barrier matrix and already at 2 Å for high barrier matrix. This very sensitive interdot distance dependence

can explain very low currents observed in the cell device with Si QDs embedded in SiO_2 matrix.[31] Thus, at least for the matrix with band offsets of 1 eV or greater, it seems unlikely that the dot-dot interaction accompanied by level splitting and miniband formation could support carrier transport due to localization unless the interdot distances are very small, on the order of one or few monolayers. The transport might proceed *via* other mechanisms, such as thermal excitation or through additional states introduced by engineered ligands attached to the dots. The
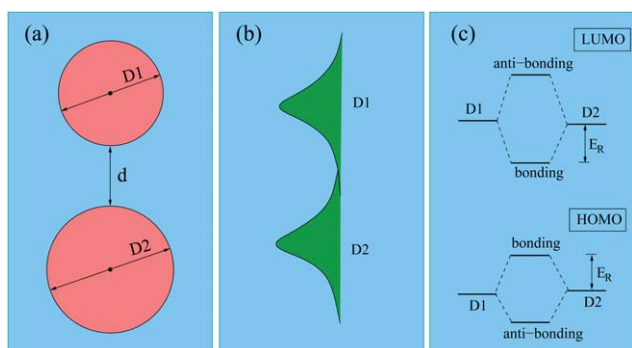
Fig. 10 Schematic electronic states interaction scheme for coupling of two dots. (a) shows the two dots with different diameters D1 and D2. The dot-dot distance is d. The coupling of two ground states localized in two dots, respectively, because of the wavefunction overlap as shown in (b) leads to level repulsion as shown in (c).

level splitting is also strongly affected by the size variations of the neighboring dots. This is demonstrated in Fig. 13 by the red, green, and blue curves that correspond to size difference between the two dots of $\Delta R/R = 0$, 10, 20%. Fig. 13 shows that dot size difference of 10 to 20% significantly reduces the level splitting. This size uniformity dependence has strong implications for carrier transport in Si QD systems such as solar cell absorber layers.

IV. Charge transport in QD solar cell

The photo-generated electron-hole pairs must be separated into free electron and hole carriers and travel to their respective negative and positive electrodes for the electrical energy to be useful. The poor carrier transport because of the carrier localization inside the dot has to be overcome in the QD solar cell design. The carrier transport in QD ensemble is further reduced due to even a small fluctuation in size, shape, and slight position shift of the individual QDs which induces
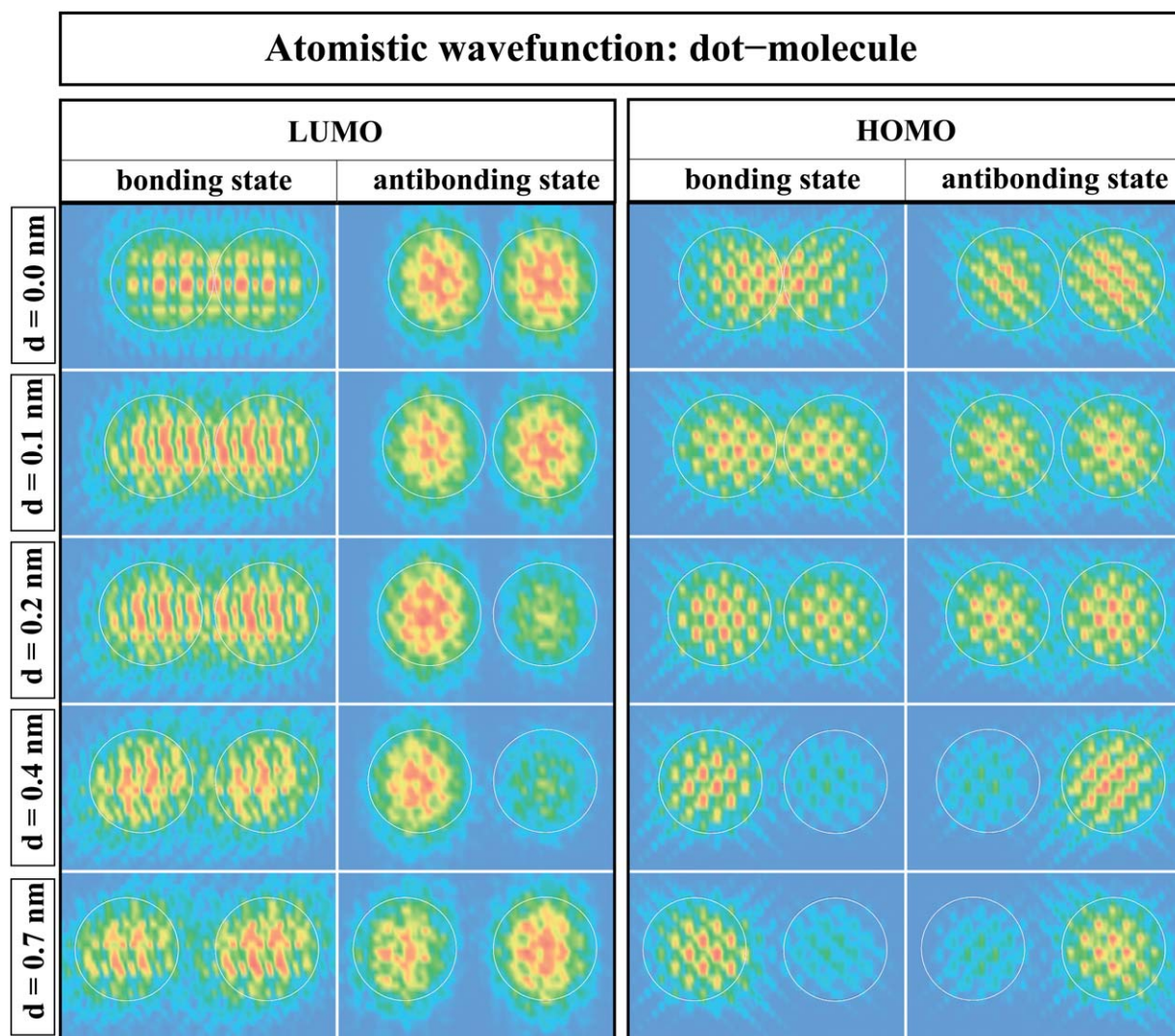
Fig. 11 Atomistic (not envelope) wavefunctions of bonding and anti-bonding states of LUMO and HOMO for Si dot-molecule ($D_1 = D_2 = 2.0$ nm) embedded in a small-gap matrix (SGM) as a function of face-to-face distance d. Numbers on above each line denote distance d.
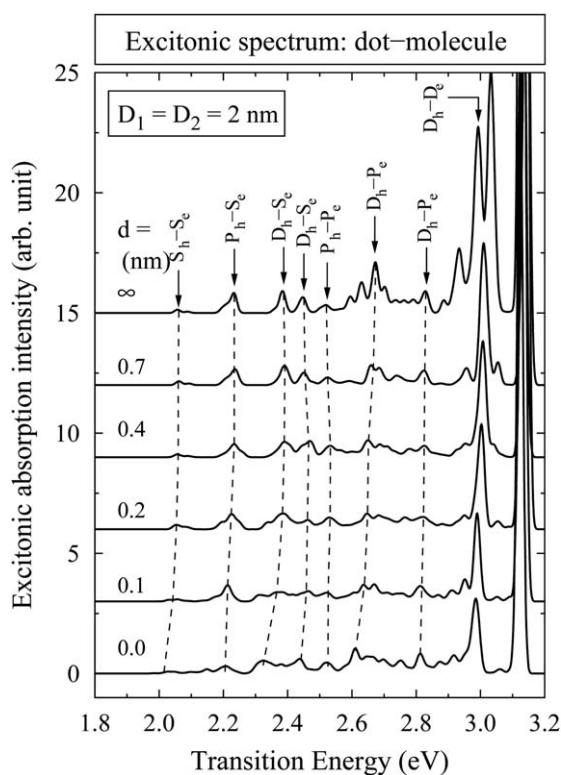
Fig. 12 Evolution of excitonic absorption spectra of a dot-molecule ($D_1 = D_2 = 2.0$ nm) embedded in a small-gap matrix (SGM) as a function of dot-dot distance d.
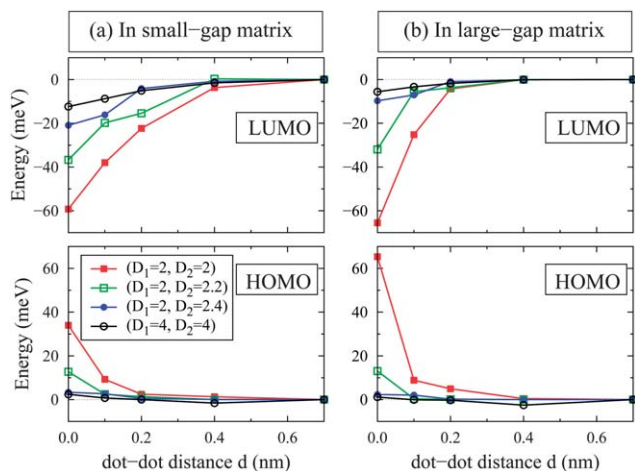
Fig. 13 Repulsion energy (E_R in Fig. 8(c)) of LUMO (top) and HOMO (bottom) of Si QD dimer embedded in (a) a small-gap matrix (SGM) and (b) in large-gap matrix (LGM) as a function of dot-dot distance d. Repulsion energy E_R defined as the LUMO (HOMO) of dot-molecule with finite d relative to that of dot-molecule with $d = \infty$.

disorder in the energy landscape. Two main mechanisms have been considered to describe carrier transport in semiconductor nanostructures:[42] transport in a miniband and hopping between Wannier–Stark states. In comparison with miniband conduction, the hopping conduction exhibits low carrier mobility $\mu \propto exp\left(-d_{ij}\right) exp\left(-\dfrac{E_i - E_j}{k_B T}\right)$ associated with two

nearest hopping sites i and j separated by distance d_{ij} with energies E_i and E_j. So far, the non-directional hopping is known to be the dominant carrier transport mechanism in QD ensemble.[43–46] The low mobility of hopping conduction results in experimentally observed extremely low carrier conductivity of QD thin films even at room temperature, such as the conductivity of ZnO QDs film is below ~1 S m⁻¹,[44] the Si QDs inside SiO_2 matrix is less than 0.001 S m⁻¹,[31] and Si QDs inside Si_3N_4 matrix can reach to 1 S/m.[31] Electron mobilities in spin-cast films of H-passivated Si QDs have been experimentally estimated in FET device and found to be very low, on the order of 10^{-5}–$10^{-6} cm^2 V^{-1} s^{-1}$.[47] Several proposals[2] have been presented to enhance the charge transport within the QD solar cells, such as using a tetrapod quantum-dot design,[2,48,49] QD embedded inside an organic polymer matrix to envision that electrons are transported by the QDs and holes are transported by the polymer,[2,50] coupling the electronic wavefunction of the electron states within QDs to the neighboring electron-accepting material,[2] and using shorter-length surface ligands.[46] However, the enhanced conductivity of QDs is still very low for the solar cell applications.

Minibands consisting of a large number of closely spaced energy levels with large wavefunction overlap between neighboring QDs facilitate efficient carrier transport in an array of QDs. Miniband conduction was observed experimentally in highly ordered and homogeneously sized InGaAs QD arrays in GaAs matrix.[51] Coherent electron transport was found in a Si QD dimer[52] as well. Thus, resonant carrier transport in minibands formed by an ordered QD array is a promising solution for QD PV. Carrier mobility due to miniband conduction in 2D superlattice is given by[42]

$$\mu = \frac{e\tau\Delta L^2}{2\hbar^2}\frac{\Delta}{4k_B T},$$ (12)

where Δ is zero-field miniband width (which is 4 times the interdot coupling T_1), L is the QD superlattice period (dot-to-dot distance plus dot diameter D), τ is the a scattering time, T is temperature, e is electron charge, and k_B and $\hbar$ are Boltzmann constant and Plank constant, respectively. Here we evaluate the possibility of resonant charge transport in Si QDs which can be extended to other materials. The miniband width Δ is proportional to the level repulsion energy E_R shown in Fig. 13. From the distance dependence of Fig. 13 we conclude that the level repulsion energy E_R decreases exponentially with increasing the dot-to-dot distance d. The miniband width Δ also decreases significantly with increasing size difference between neighboring dots. According to eqn (12) the miniband conduction mobility $\mu \propto \Delta$ and will be also even exponentially reduced with increasing the dot-to-dot distance or disorder in QD sizes. We conclude that in order to realize effective dot-dot carrier transport *via* miniband mechanism, one needs to produce Si dot arrays within about 10% size tolerance which is a rather difficult task at the present stage (although PbS and CdSe have satisfied this with solution chemistry[43,53]) and dots have to be as close as possible.

Finally, we address the question of whether the photocarriers in Si QD arrays are transported as charges or as bound excitons. The exciton binding energy Si dots increases with decreasing the size and is governed by the of quantum-confined PL bandgap (see Fig. 4 and discussion of Section B). Remarkably, this

dependence is not affected by the matrix bandgap. At the PL bandgap of 2 eV that corresponds to 2 nm size dots in 3.2 eV matrix, and about 2.8 nm dots in 5.9 eV matrix, the exciton binding energy is about 200 meV. Such a considerable binding energy resembles that observed in organic semiconductors and is expected to affect the charge separation.[34] We have to note, however, that the exciton binding energies are likely to be lower in dense arrays of Si dots as compared to isolated dots in matrix, due to higher average dielectric constant introduced by the Si dots. At present, however, Si QD volume fractions in experimentally grown films (e.g. with Si particles embedded into SiO2 matrix) are relatively low. This, along with the negligible dot-dot interaction as supported by data of Fig. 8 and 9 at the surface-surface distances typically found in those films (~1 nm), might provide a possible explanation of poor carrier collection achieved experimentally so far. Closely-packed Si QD arrays might be necessary to reduce the exciton binding energy. Alternatively, Si QDs in combination with materials/structures that facilitate exciton dissociation (such as Si QD/P3HT hybrid absorber layers,[50] might enable advantages of excitonic effects.

V. Summary

By performing atomistic calculation including many-body interaction we have studied the important PV-related critical quantities from absorption to transport for Si QDs solar cell. First, we find that the low-efficient absorption in bulk indirect Si is significantly enhanced in Si QDs, specially for small dot sizes, due to quantum-confinement induced $\Gamma - X$ coupling. Second, the quantum confinement effect has detrimental effects on PV applications, such as it significantly enhances the exciton binding energy in Si QDs leading to charge separation difficulty. We observe an universal linear function of binding energy versus excitonic gap for all Si QDs. This universal linear function is very helpful for obtaining experimentally the exciton binding energy of Si QDs by just measuring the excitonic gap without any knowledge on dot shape, size, and surface treatment. Third, we evaluate the possibility of resonant charge transport in an array of Si QDs via additional miniband channels created by dot-dot coupling. We have shown that for such charge transport the Si QDs embedded into a matrix should have tight size tolerances and be very closely spaced, up to an intimate contact. Fourth, the loss of quantum confinement effect induced by dot-dot coupling is negligible. The lost quantum confinement energy is smaller than 70 meV even for two dots upon intimate contact relative to an isolated single dot. Furthermore, we also demonstrate that the symmetry effects also play an important role on bandgap and absorption spectrum of Si QDs. This work provides some valuable guidelines for experimental methods of growing, assembling, and functionalizing the Si QDs into a PV absorber layer material. The results obtained from Si QDs can be extended to other QD materials.

Acknowledgements

References

1 A. J. Nozik, *Phys. E.*, 2002, **14**, 115; A. J. Nozik, *Nano Lett.*, 2010, **10**, 2735.
2 G. E. Jabbour and D. Doderer, *Nat. Photonics*, 2010, **4**, 604.
3 J. Nelson, *The Physics of Solar Cells*, Imperial College press, 2003.
4 R. Leon, G. M. Swift, B. Magness, W. A. Taylor, Y. S. Tang, K. L. Wang, P. Dowd and Y. H. Zhang, *Appl. Phys. Lett.*, 2000, **76**, 2074.
5 A. J. Nozik, *Phys. E.*, 2002, **14**, 115; R. D. Schaller and V. I. Klimov, *Phys. Rev. Lett.*, 2004, **92**, 186601; R. J. Ellingson, M. C. Beard, J. C. Johnson, P. Yu, O. I. Micic, A. J. Nozik, A. Shabaev and A. L. Efros, *Nano Lett.*, 2005, **5**, 865; J. W. Luo, A. Franceschetti and A. Zunger, *Nano Lett.*, 2008, **8**, 3174.
6 J. W. Luo and A. Zunger, *Phys. Rev. Lett.*, 2010, **105**, 176805.
7 L. W. Wang, *Phys. Rev. B: Condens. Matter*, 2000, **61**, 7241.
8 H. Fu, L. W. Wang and A. Zunger, *Appl. Phys. Lett.*, 1997, **71**, 3433.
9 A. Zunger, in *Quantum Theory of Real Materials*, ed J. R. Chelikowsky and S. G. Louie, Kluwer, Boston, 1996, p. 173.
10 J. W. Luo, A. N. Chantis, M. van Schilfgaarde, G. Bester and A. Zunger, *Phys. Rev. Lett.*, 2010, **104**, 066405.
11 C. Pryor, J. Kim, L. W. Wang, A. J. Williamson and A. Zunger, *J. Appl. Phys.*, 1998, **83**, 2548.
12 R. W. Godby, M. Schlüter and L. J. Sham, *Phys. Rev. Lett.*, 1986, **56**, 2415.
13 M. S. Hybertsen and S. G. Louie, *Phys. Rev. B*, 1986, **34**, 5390.
14 J. W. Luo, A. Franceschetti and A. Zunger, *Nano Lett.*, 2009, **9**, 2648.
15 A. Franceschetti, H. Fu, L. W. Wang and A. Zunger, *Phys. Rev. B: Condens. Matter*, 1999, **60**, 1819.
16 L. W. Wang and A. Zunger, *Phys. Rev. B: Condens. Matter*, 1995, **51**, 17398.
17 L. Kleinman and D. M. Bylander, *Phys. Rev. Lett.*, 1982, **48**, 1425.
18 G. Bester, S. Nair and A. Zunger, *Phys. Rev. B: Condens. Matter*, 2003, **67**, 161306.
19 Semiconductors: Group IV Elements, IV–IV and III–V Compunds, *Landolt-Börnstein, New Series, Group III*, Vol. 41, Pt. A, ed. U. Rössler, Springer-Verlag, Berlin, 2001.
20 A. Puzder, A. J. Williamson, J. C. Grossman and G. Galli, *Phys. Rev. Lett.*, 2002, **88**, 097401.
21 A. Gali, M. Vrs, D. Rocca, G. T. Zimanyi and G. Galli, *Nano Lett.*, 2009, **9**, 3780; D. X. Li and J. Y. Feng, *Appl. Phys. Lett.*, 2008, **92**, 243117; Z. Wu, J. B. Neaton and J. C. Grossman, *Nano Lett.*, 2009, **9**, 2418; X. Zhao, C. M. Wei, L. Yang and M. Y. Chou, *Phys. Rev. Lett.*, 2004, **92**, 236805.
22 M. V. Wolkin, J. Jorne, P. M. Fauchet, G. Allan and C. Delerue, *Phys. Rev. Lett.*, 1999, **82**, 197.
23 L. W. Wang and A. Zunger, *J. Chem. Phys.*, 1994, **100**, 2394.
24 J. Shumway, A. Franceschetti and A. Zunger, *Phys. Rev. B: Condens. Matter*, 2001, **63**, 155316.
25 Although the real SiO2 has a much larger band gap (~9 eV) than that of fitted small-gap matrix (3.2 eV), the latter reproduces well the excitonic gap of the Si QDs embedded in the former. The main reason of this surprising agreement is that the kinetic energy (or quantum confinement energy) of electron states in QD is determined not only by well potential (bandoffset) but also by other factors[20,54] e.g., effective mass mismatch at interface between dot material and matrix.[26]
26 J. W. Luo, S. S. Li, J. B. Xia and L. W. Wang, *Appl. Phys. Lett.*, 2006, **88**, 143108.
27 B. G. Fernandez, M. López, C. García, A. Pérez-Rodríguez, J. R. Morante, C. Bonafos, M. Carrada and A. Claverie, *J. Appl. Phys.*, 2002, **91**, 798–807.
28 G. Ledoux, J. Gong, F. Huisken, O. Guillois and C. Reynaud, *Appl. Phys. Lett.*, 2002, **80**, 4834.
29 T. Y. Kim, N. M. Park, K. H. Kim, G. Y. Sung, Y. W. Ok, T. Y. Seong and C. J. Choi, *Appl. Phys. Lett.*, 2004, **85**, 5355.
30 Y. Kanemitsu, S. Okamoto, M. Otobe and S. Oda, *Phys. Rev. B: Condens. Matter*, 1997, **55**, R7375.
31 G. Conibeer, et al., *Thin Solid Films*, 2006, **511 & 512**, 654; G. Conibeer, et al., *Thin Solid Films*, 2008, **516**, 6748; G. Conibeer, Third Generation Photovoltaics: Silicon nanostructure & Hot Carrier solar cells, *GCEP Research Symposium*, Stanford University, Oct 1–3, 2008; G. Conibeer, et al., Silicon quantum dot based solar cells: addressing the issues of doping, voltage and current transport, *Prog. Photovoltaics*, 2010, DOI: 10.1002/pip.1045.

32 S. Takeoka, M. Fujii and S. Hayashi, *Phys. Rev. B: Condens. Matter*, 2000, **62**, 16820.
33 F. Meillaud, A. Shah, C. Droz, E. Vallat-Sauvain and C. Miazza, *Sol. Energy Mater. Sol. Cells*, 2006, **90**, 2952.
34 B. A. Gregg, *J. Phys. Chem. B*, 2003, **107**, 4688.
35 G. D. Scholes and G. Rumbles, *Nat. Mater.*, 2006, **5**, 683.
36 F. A. Reboredo, A. Franceschetti and A. Zunger, *Phys. Rev. B: Condens. Matter*, 2000, **61**, 13073.
37 A. Franceschetti, A. Williamson and A. Zunger, *J. Phys. Chem. B*, 2000, **104**, 3398.
38 K. Nishiguchi, X. Zhao and S. Odaa, *J. Appl. Phys.*, 2002, **92**, 2748.
39 M. Sykora, L. Mangolini, R. D. Schaller, U. Kortshagen, D. Jurbergs and V. I. Klimov, *Phys. Rev. Lett.*, 2008, **100**, 067401.
40 G. M. Dalpian, M. L. Tiago, M. L. del Puerto and J. R. Chelikowsky, *Nano Lett.*, 2006, **6**, 501.
41 S. V. Goupalov, *Phys. Rev. B*, 2009, **79**, 23305.
42 H. T. Grahn, K. von Klitzing, K. Ploog and G. H. Döhler, *Phys. Rev. B: Condens. Matter*, 1991, **43**, 12094.
43 D. V. Talapin, J. S. Lee, M. V. Kovalenko and E. V. Shevchenko, *Chem. Rev.*, 2010, **110**, 389.
44 A. J. Houtepen, D. Kockmann and D. Vanmaekelbergh, *Nano Lett.*, 2008, **8**, 3516.
45 M. S. Kang, A. Saku, D. J. Norris and C. D. Frisbie, *Nano Lett.*, 2010, **10**, 3727.
46 Y. Liu, M. Gibbs, J. Puthussery, S. Gaik, R. Ihly, H. W. Hillhouse and M. Law, *Nano Lett.*, 2010, **10**, 1960.
47 Z. C. Holman, C. Liu and U. R. Kortshagen, *Nano Lett.*, 2010, **10**, 2661.
48 B. Sun, E. Marx and N. C. Greenham, *Nano Lett.*, 2003, **3**, 961.
49 S. Dayal, N. Kopidakis, D. C. Olson, D. S. Ginley and G. Rumbles, *Nano Lett.*, 2010, **10**, 239.
50 C. Y. Liu, Z. C. Holman and U. R. Kortshagen, *Nano Lett.*, 2009, **9**, 449.
51 H. Z. Song, K. Akahane, S. Lan, H. Z. Xu, Y. Okada and M. Kawabe, *Phys. Rev. B: Condens. Matter*, 2001, **64**, 085303.
52 L. P. Rokhinson, L. J. Guo, S. Y. Chou, D. C. Tsui, E. Eisenberg, R. Berkovits and B. L. Altshuler, *Phys. Rev. Lett.*, 2002, **88**, 186801.
53 J. M. Luther, J. Gao, M. T. Lloyd, O. E. Semonin, M. C. Beard and A. J. Nozik, *Adv. Mater.*, 2010, **22**, 3704.
54 S. Kilina, S. Ivanov and S. Tretiak, *J. Am. Chem. Soc.*, 2009, **131**, 7717.